

UC Berkeley

UC Berkeley Previously Published Works

Title

Atomically Dispersed Platinum in Surface and Subsurface Sites on MgO Have Contrasting Catalytic Properties for CO Oxidation

Permalink

<https://escholarship.org/uc/item/30q7z35d>

Journal

The Journal of Physical Chemistry Letters, 13(17)

ISSN

1948-7185

Authors

Chen, Yizhen
Rana, Rachita
Huang, Zhennan
[et al.](#)

Publication Date

2022-05-05

DOI

10.1021/acs.jpcllett.2c00667

Peer reviewed

Atomically Dispersed Platinum in Surface and Subsurface Sites on MgO Have Contrasting Catalytic Properties for CO Oxidation

Yizhen Chen,[○] Rachita Rana,[○] Zhennan Huang, Fernando D. Vila, Tyler Sours, Jorge E. Perez-Aguilar, Xiao Zhao, Jiyun Hong, Adam S. Hoffman, Xu Li, Chunyan Shang, Thomas Blum, Jie Zeng, Miaofang Chi, Miquel Salmeron, Coleman X. Kronawitter,* Simon R. Bare,* Ambarish R. Kulkarni,* and Bruce C. Gates*



Cite This: *J. Phys. Chem. Lett.* 2022, 13, 3896–3903



Read Online

ACCESS |



Metrics & More

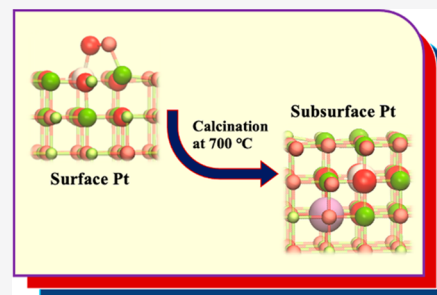


Article Recommendations



Supporting Information

ABSTRACT: Atomically dispersed metals on metal oxide supports are a rapidly growing class of catalysts. Developing an understanding of where and how the metals are bonded to the supports is challenging because support surfaces are heterogeneous, and most reports lack a detailed consideration of these points. Herein, we report two atomically dispersed CO oxidation catalysts having markedly different metal–support interactions: platinum in the first layer of crystalline MgO powder and platinum in the second layer of this support. Structural models have been determined on the basis of data and computations, including those determined by extended X-ray absorption fine structure and X-ray absorption near edge structure spectroscopies, infrared spectroscopy of adsorbed CO, and scanning transmission electron microscopy. The data demonstrate the transformation of surface to subsurface platinum as the temperature of sample calcination increased. Catalyst performance data demonstrate the lower activity but greater stability of the subsurface platinum than of the surface platinum.



Atomically dispersed noble metals on supports offer new catalytic properties as well as efficient use of the metals, but there is a lack of understanding of how these properties depend on the structures of the anchoring sites and the metal–support bonding.^{1–4} Atomically dispersed supported metals are more nearly uniform than typical supported metal catalysts and therefore offer better opportunities for fundamental understanding.^{1–4} *In operando* spectroscopies and high-resolution imaging have emerged as the most informative characterization methods,^{3,5–11} but the characterization challenges are formidable, complicated by the support surface heterogeneity and the strong tendency of atomically dispersed noble metals to be converted into metal clusters/nanoparticles under reducing conditions.^{11,12} In most of the reported work with atomically dispersed metals on metal oxide supports, the nature of the metal–support bonding has been overlooked, and only a few reports have recognized the importance of metal atoms occupying subsurface positions in supports.^{13–15}

Herein, we report results of X-ray absorption spectroscopy (XAS), atomic-resolution electron microscopy, and density functional theory (DFT) calculations that demonstrate two distinct sites for atomically dispersed platinum on MgO. In addition to a recently reported site¹³ for bonding platinum in the second layer of MgO—within the lattice—we now report platinum in a more accessible site in the first MgO layer. This newly discovered site is characterized by relatively high catalytic activity for CO oxidation but low stability. Further,

we show that high-temperature calcination drives the platinum from the first MgO layer irreversibly into the second layer, where it is more stably bonded but barely accessible. These results demonstrate trade-offs between catalytic activity and stability.

Pt/MgO₄₀₀ (the subscript is the calcination temperature in °C) was synthesized from K₂PtCl₄ slurried with MgO powder in ethanol–water solutions, then dried, and calcined in 20% O₂ in N₂ at 400 °C (Supporting Information).¹³ Low metal loadings (≈0.05 wt %) were used in an attempt to minimize the number of different bonding sites for platinum on the support. Some of the Pt/MgO₄₀₀ samples were subsequently calcined under more severe conditions, at 700 °C, giving Pt/MgO₇₀₀.

Transmission electron microscopy (TEM) images and X-ray diffraction (XRD) patterns show that the MgO was present as the cubic phase, consisting of ~100 nm diameter crystallites; there was no evidence of crystalline metallic platinum or PtO₂ (Figure S1). Infrared (IR) bands of MgO surface OH groups

Received: March 7, 2022

Accepted: April 22, 2022

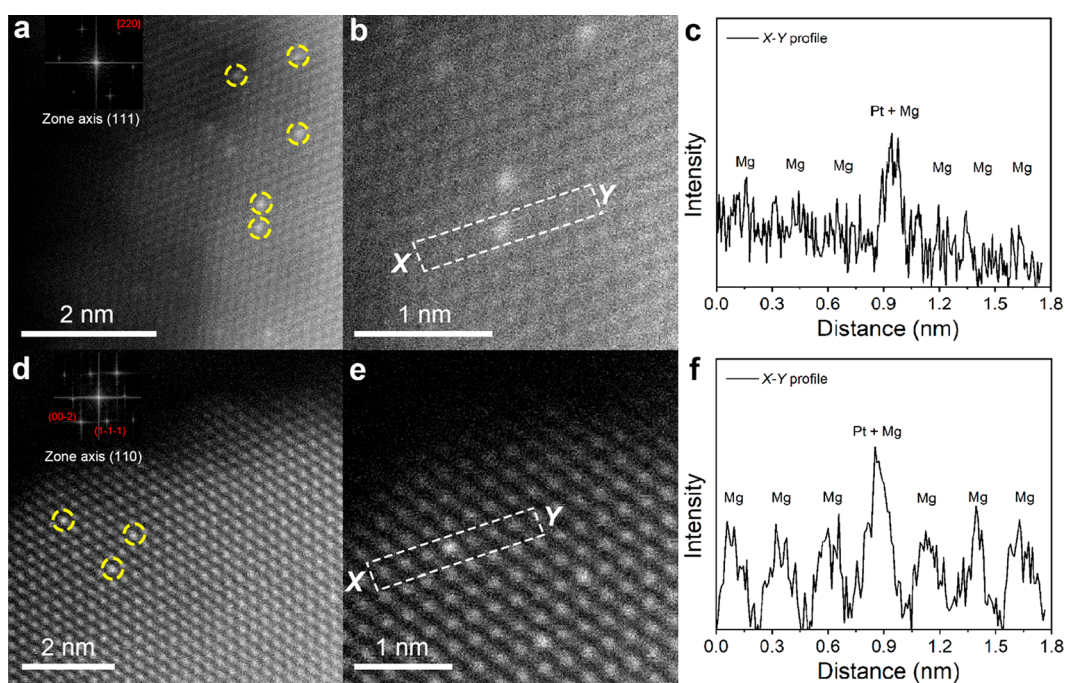


Figure 1. (a) HAADF-STEM image of Pt/MgO₄₀₀ along the (111) zone axis. Platinum atoms are highlighted in yellow circles; the inset shows the corresponding fast Fourier transform (FFT) pattern. (b) Magnified HAADF-STEM image of Pt/MgO₄₀₀. (c) Intensity profile along the X–Y axis in (b). (d) HAADF-STEM image of Pt/MgO₇₀₀ along the (110) zone axis. Platinum atoms are highlighted in yellow circles; the inset shows the corresponding FFT pattern. (e) Magnified HAADF-STEM image of Pt/MgO₇₀₀. (f) Intensity profile along the line X–Y axis in (e).

(at 3766 and 3726 cm^{-1}) decreased in intensity as the calcination temperature increased to 700 °C (Figure S2); the resultant MgO was highly dehydroxylated.^{6,13} O 1s X-ray photoelectron spectroscopy (XPS) peaks at 529.8 and 532.0 eV provide evidence of oxygen atoms in the MgO lattice and surface OH groups, respectively (Figure S3).^{16–18} The intensity of the 532.0 eV peak characterizing Pt/MgO₇₀₀ is less than that characterizing Pt/MgO₄₀₀, consistent with IR data showing that MgO dehydroxylation took place during calcination (Figure S4 and Table S1). BET surface area measurements are consistent with these results.¹⁹

High-angle annular dark field (HAADF)-scanning TEM (STEM) images, Figure 1, show the presence of atomically dispersed platinum and the absence of clusters/nanoparticles in both Pt/MgO₄₀₀ and Pt/MgO₇₀₀. The bright spots in yellow circles in Figure 1a,d are illustrative, clearly showing that isolated platinum atoms are located atop or nearly atop columns of Mg cations along a zone axis.¹³ Intensity profiles along the X–Y lines in the images of Figure 1b,e reinforce the conclusions (Figure 1c,f).

To investigate the local bonding environments of the platinum in these two samples, we used XAS, with *in operando* spectra recorded at the platinum L_{III} edge during the calcination as the temperature was ramped at 5 °C/min from room temperature to 700 °C with the sample in 20% O₂ in helium flowing at a rate of 20 mL(NTP)/min. The X-ray absorption near edge structure (XANES) spectra include isosbestic points, indicating that the changes were stoichiometrically simple (Figure 2a and Figure S5). The white line intensity at the platinum L_{III} edge characterizing the sample at room temperature in flowing helium, recorded after the 700 °C calcination, is markedly greater than that of the initial sample (Figure 2b), implying that the platinum species with lower

oxidation state used in the synthesis was oxidized during the subsequent calcination.

Extended X-ray absorption fine structure (EXAFS) spectra at the platinum L_{III} edge were recorded to determine the local bonding environment of the platinum before and after calcination (Figure 2e,f). Analysis of the data characterizing Pt/MgO₄₀₀ was performed with a fitting procedure (referred to as QuantEXAFS)^{13,20} that included all the relevant scattering paths in structures determined to be plausible by DFT.²¹ The candidate models in the database included 47 DFT-optimized structures. The temperature-dependent phase diagram was constructed (using pMuTT, harmonic approximation for vibrational entropy) for each site (Figure S6).^{13,21–23} The DFT-optimized geometries (Figure 2c) and corresponding best fits of the data (Figure 2e and Table 1) indicate average Pt–O and Pt–Mg coordination numbers ($\text{CN}_{\text{Pt-O}}$ and $\text{CN}_{\text{Pt-Mg}}$) of 6 and 8, respectively. The model that agrees best with the data, [100]/sub0/*O₂ (Figure 2e and Table 1—see caption of Figure 2 for explanation of notation), corresponds to isolated platinum atoms on the stoichiometric [100] surface and bonded to five oxygen atoms of the MgO support and one oxygen atom inferred to have formed from O₂ in the calcination treatment. In contrast, the data characterizing the sample calcined at 700 °C, PtMgO₇₀₀, which were analyzed by the above-mentioned method (as already reported¹³), show that platinum was present in the first subsurface layer located in the [100] MgO facet at Mg vacancy sites, with the coordination numbers $\text{CN}_{\text{Pt-O}}$ and $\text{CN}_{\text{Pt-Mg}}$ being 6 and 11, respectively (Figure 2f and Table 1). The corresponding DFT-optimized geometries ([100]^{Mg-vac}/sub1) are shown in Figure 2d. Candidate EXAFS models that included a Pt–Pt scattering path led to nonsensical results indicating that there was no evidence of platinum clusters or nanoparticles.

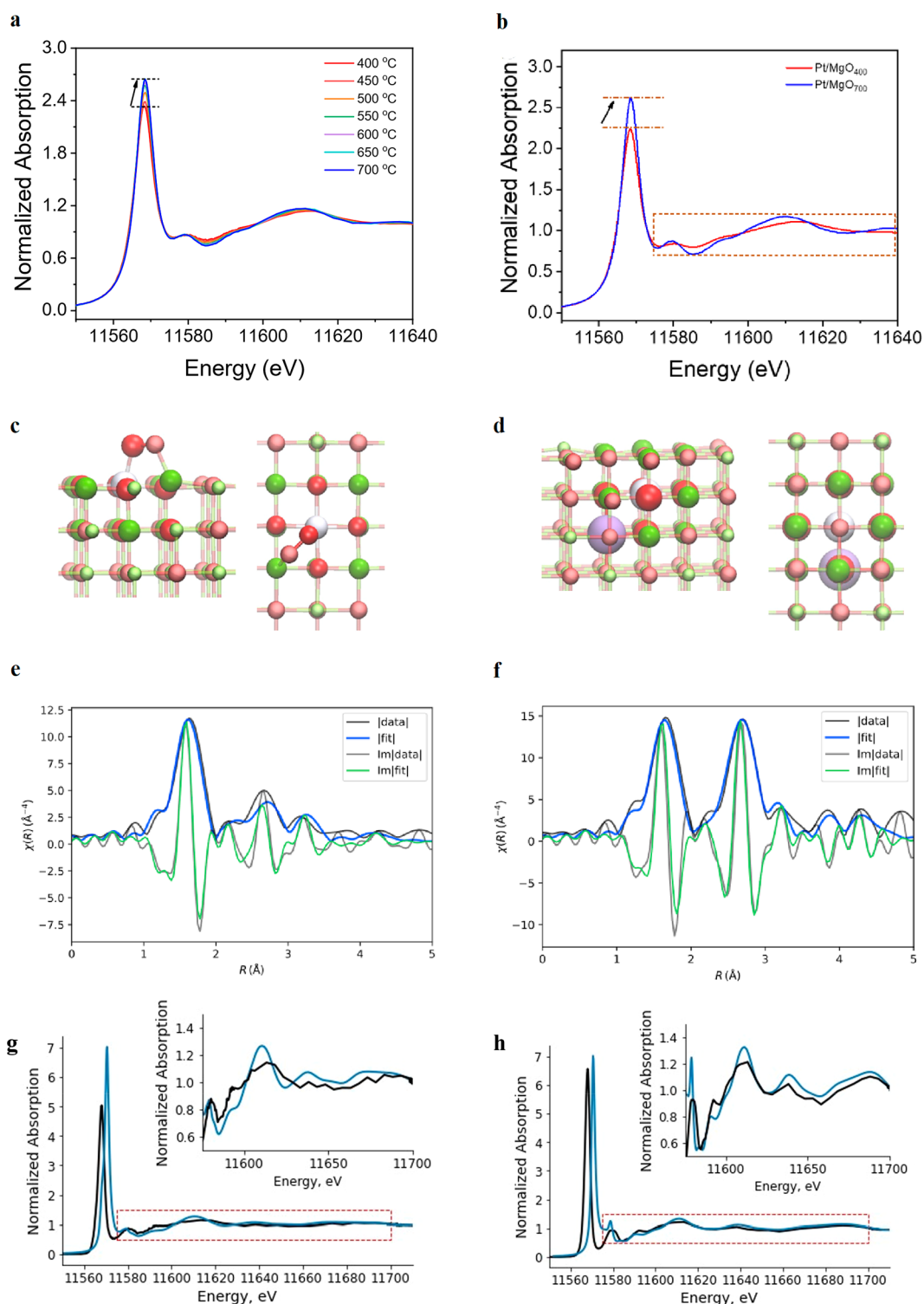
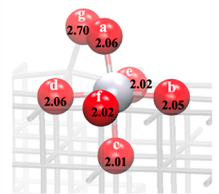
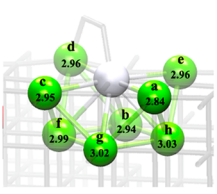
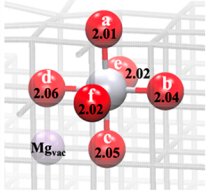
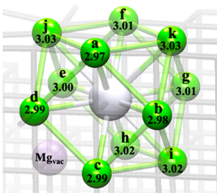


Figure 2. (a) Conventional XANES spectra characterizing Pt/MgO at various temperatures, representing structural changes taking place during calcination. The sample was heated from room temperature to 700 °C at a rate of 5 °C/min as the sample was exposed to 20% O₂ in helium flowing at a rate of 20 mL(NTP)/min for 0.5 h. (b) XANES spectra characterizing Pt/MgO₄₀₀ and Pt/MgO₇₀₀, each in helium flowing at 20 mL(NTP)/min at room temperature. The DFT-optimized geometries of the most stable (c) surface structure [100]^{Mg-vac}/sub0/*O₂ side view and top view and (d) subsurface structure [100]^{Mg-vac}/sub1 side view and top view. EXAFS spectra characterizing (e) Pt/MgO₄₀₀ and (f) Pt/MgO₇₀₀ in helium flowing at 20 mL (NTP)/min at room temperature in *R*-space (*k*³-weighted) with the corresponding EXAFS fits based on [100]/sub0/*O₂ and [100]^{Mg-vac}/sub1 structures, respectively, showing the magnitude (fit: blue; experiment: black) and imaginary portions (fit: green; experiment: black) of Fourier transforms of the data. The *k*-range of 2.2–12.5 Å⁻¹ and the *R*-range of 1.0–5.0 Å were used for the fits. Colors: Mg (green), O (red), and Pt (gray) (The nearest neighbors of Pt are shown in bright colors, and the other atoms are shown in faded colors.). The purple sphere represents the subsurface magnesium vacancy. Simulated (blue) and experimental (black) HERFD-XANES spectra of (g) Pt/MgO₄₀₀ in helium flowing at 20 mL (NTP)/min at room temperature determined for the best-fit EXAFS data from the DFT-optimized structure [100]/sub0/*O₂ and (h) Pt/MgO₇₀₀ in helium flowing at 20 mL (NTP)/min at room temperature determined for the best-fit DFT structure [100]^{Mg-vac}/sub1.

Table 1. EXAFS Fitting Parameters for Pt/MgO₄₀₀ and Pt/MgO₇₀₀ Modeled Using QUANTEXAFS with the Respective Structures with the Pt–O and Pt–Mg Coordination Numbers^a

Sample	Structures	ΔE_0 (eV)	$10^3 \times \sigma_i^2$ (\AA^2)	
Pt/MgO ₄₀₀		7.9 ± 1.3	Pt-O (7)	1.1 ± 0.5
			Pt-Mg (8)	1.3 ± 3.2
Pt/MgO ₇₀₀		5.8 ± 1.6	Pt-O (6)	4.0 ± 1.1
			Pt-Mg (11)	4.9 ± 1.1

^aThe numbers on the spheres represent Pt–O and Pt–Mg bond distances in \AA . Color scheme: O (red), Pt (gray), Mg (green), and Mg-vac (purple). Notation: ΔE_0 is the energy alignment parameter, and σ is the disorder term.

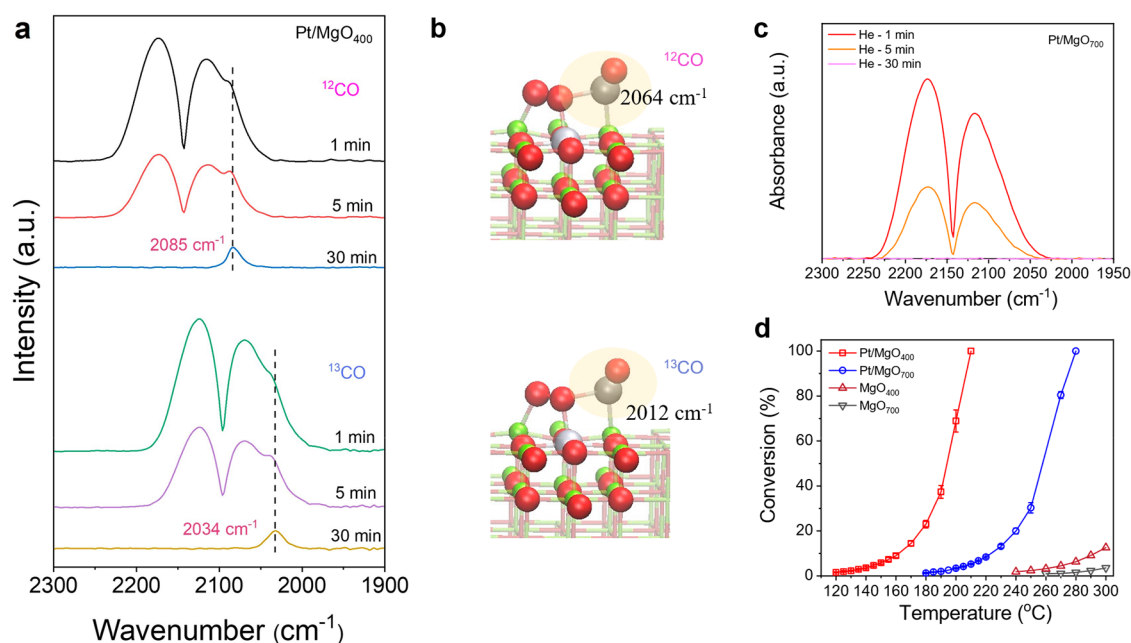


Figure 3. (a) IR spectra in the ν_{CO} region characterizing Pt/MgO₄₀₀ recorded after the sample had been in contact with flowing 10% CO in helium for 30 min, followed by a purge of the IR cell with helium for 1, 5, and 30 min. After each of these treatments, IR spectra were recorded after exposure of the sample to a 2 min pulse of flowing ¹³CO, followed by a purge of the IR cell with the helium for 1, 5, and 30 min. (b) Calculated positions of peaks for possible CO and ¹³CO adsorbed on the [100]/sub0/*O₂ structure. (c) IR spectra in the ν_{CO} region characterizing Pt/MgO₇₀₀ recorded after the sample had been in contact with flowing 10% CO in helium for 30 min, followed by a purge of the IR cell with helium for 1, 5, and 30 min. (d) Light-off curves characterizing CO oxidation catalyzed by Pt/MgO₄₀₀ and Pt/MgO₇₀₀. Error bars represent standard deviations determined from three independent measurements. The once-through plug-flow reactor was heated from room temperature to 300 °C at a rate of 2 °C/min. The feed was 5.0% CO in helium flowing at 4.0 mL (NTP)/min + 5.0% O₂ in helium flowing at 16.0 mL (NTP)/min; the catalyst mass in each experiment was 100 mg (Data characterizing the supports MgO₄₀₀ and MgO₇₀₀ are shown for comparison.).

The central point shown by comparing the EXAFS data characterizing the two differently calcined samples is that the Pt–O and Pt–Mg coordination numbers changed significantly as the calcination temperature increased from 400 to 700 °C, and the location of platinum changed from a bonding site in the first MgO layer to a bonding site in the second MgO layer.

To gain further insight into the structures and to help overcome the limitations associated with core-hole lifetime broadening in conventional XANES spectroscopy,^{24,25} we also

collected high energy resolution fluorescence detection (HERFD)-XANES data. These data, when combined with simulated spectra, provide additional insight into the structure of the supported platinum. The HERFD-XANES data were compared with FEFF-simulated XANES spectra calculated from the above-mentioned DFT-optimized geometries (Figure 2g,h).^{13,26,27} The structure [100]/sub0/*O₂ is in good agreement with the HERFD-XANES data characterizing this sample (Figure 2g), with a Fréchet distance of 0.155. (Fréchet

distances have been used previously to quantify the similarity between the experimental and simulated spectra.¹³ Further, the structure of $[100]_{\text{Mg-vac}}^{\text{sub1}}$ is in good agreement with the HERFD-XANES results characterizing Pt/MgO₇₀₀, as we reported before (Figure 2h).¹³ Details are presented in Figure S7.

The oxidation state of platinum in the subsurface sites, determined from DFT calculations using Bader charge analysis¹³ ($q_{\text{Bader}} = +1.35e$), is close to that of Pt⁴⁺ in H₂Pt(OH)₆ ($q_{\text{Bader}} = +1.41e$). Comparable calculations showed that the oxidation state of platinum in the first MgO layer ($q_{\text{Bader}} = +1.17e$) is between those of Pt²⁺ ($q_{\text{Bader}} = +0.86e$ for Pt(acetylacetonato)₂) and Pt⁴⁺ and thus lower than that of platinum in the second layer. These results are in good agreement with the XANES data showing that the white line intensity increased as the calcination temperature was raised from 400 to 700 °C (Figure 2a,b,g,h), and they are in good agreement with XANES data characterizing reference compounds (Figure S8).

To repeat for emphasis: a comparison of the results determined for the samples calcined at 400 and at 700 °C shows that during the calcination as the temperature was raised to 700 °C, in the interval from 400 to 700 °C, the atomically dispersed platinum was converted from surface to subsurface species.

The platinum in the subsurface sites is clearly characterized by stronger metal–support interactions than platinum in the surface sites, lacking sites with coordinative unsaturation to react directly with adsorbates such as CO at room temperature and requiring reaction steps such as removal of a surface oxygen atom for CO oxidation catalysis, as discussed in the reported work.¹³ The results of locally projected density of states calculations shown in Figure S7 bolster the conclusion.

The expectation that the different surroundings of the platinum in Pt/MgO₄₀₀ and Pt/MgO₇₀₀ are characterized by markedly different reactivities was confirmed by IR spectra of samples exposed to CO. CO was adsorbed on Pt/MgO₄₀₀ at room temperature and found to be characterized by a band at 2085 cm⁻¹ (Figure 3a), with a full width at half-maximum (fwhm) value of only 17 cm⁻¹, which is assigned to CO on atomically dispersed Pt^{δ+}.²⁸ The narrowness of the band implies that the species were nearly uniform in structure.²⁹ This band shifted to 2034 cm⁻¹ when the sample at room temperature was exposed to ¹³CO, as this ligand displaced ¹²CO; the frequencies are consistent with the harmonic approximation and confirm the identification of terminally bonded CO on the platinum (Figure 3a).³⁰ These results are confirmed by the DFT-predicted ¹²CO and ¹³CO frequencies (Figure 3b, Figure S9, and Table S2).^{24,31}

In sharp contrast to these results, the IR spectra provide no evidence of room-temperature CO adsorption on the sample with the subsurface platinum (Figure 3c).¹³ Thus, the IR data are in good agreement with the XAS data showing that the highly coordinated Pt⁴⁺ species in the second layer of MgO ($[100]_{\text{Mg-vac}}^{\text{sub1}}$) were less accessible to reactants than those in the first layer ($[100]_{\text{sub0}}^{\text{O}_2}$).

These two samples incorporating differently coordinated platinum were compared as catalysts for CO oxidation in a conventional once-through plug-flow reactor operated at atmospheric pressure; the CO/O₂ molar ratio in the feed was 1:4 (Figure 3d). As the temperature of Pt/MgO₄₀₀ in the reactor was ramped from room temperature at a rate of 2 °C/min, CO oxidation activity was first observed at about 120 °C

(and the CO conversion approached 100% at 210 °C). When the catalyst was Pt/MgO₇₀₀, a much higher temperature was required for the onset of catalysis, 180 °C (Figure 3d).¹³

After use in three comparable independent catalysis experiments, the Pt/MgO₄₀₀ sample was exposed to CO and characterized by IR spectroscopy (Figure S10). The band at 2085 cm⁻¹, which is characteristic of CO on atomically dispersed platinum,²⁸ was still evident, but it was now accompanied by a broad absorption centered at 2056 cm⁻¹, which is assigned to CO adsorbed on metallic platinum (Figure S10).³² The assignment of these bands as carbonyl bands was confirmed by the band shifts when each sample at room temperature was exposed to ¹³CO, which was observed to replace ¹²CO ligands on the platinum (Figure S10).

STEM images of the Pt/MgO₄₀₀ after use as a catalyst and EXAFS spectra recorded during catalysis confirm that the platinum sintered (Figure S11, Figure S12 and Figure S13), evidently having been reduced by CO and having migrated on the support surface, forming metallic platinum species. These results are consistent with prior observations of cluster formation from atomically dispersed supported platinum (or palladium) catalysts during CO oxidation,^{33,34} implying that the atomically dispersed platinum in Pt/MgO₄₀₀ is not stable under CO oxidation conditions and that the catalytically active species were present in a mixture of atomically dispersed and metallic platinum; the data are consistent with attribution of the catalytic activity in that sample to the metallic platinum.

In contrast to these results, the IR data characterizing platinum in the subsurface sites remained unchanged after catalysis (Figure S14).¹³ These less accessible platinum atoms were not only much less active catalytically than those in the first MgO layer but also much more resistant to sintering than the platinum in the first MgO layer, as shown by reported XAS, IR, and STEM data characterizing the used subsurface platinum catalyst.¹³

Trade-offs between high catalytic activity and structural stability are common in catalysis, often explained by roles of ligands stabilizing a metal center but limiting access of reactants to that center. Thus, coordinative unsaturation at metal centers is needed to allow bonding of reactants. The results reported here show that the platinum in the second layer of MgO is markedly less reactive with CO than the platinum in the first layer and correspondingly less active as a catalyst for CO oxidation. However, the platinum in the subsurface sites is much more stable—resistant to sintering—than the platinum in the first layer. The data point to a trade-off between activity and stability of these catalysts and lead one to reflect on a rough analogy to homogeneous organometallic catalysis, illustrated by olefin hydroformylation with rhodium complexes, whereby increased encumbrance (ligation) of a rhodium center leads to lower activity but a higher selectivity for aldehyde formation.^{35,36}

The observation of atomically dispersed platinum atoms not only in the first MgO layer but also in the second layer calls to mind reports of atomically dispersed supported metals in which the metals have been regarded as support-embedded.^{37–39} The literature includes many examples of doped solid catalysts, with dopants in various and difficult-to-determine subsurface sites.^{40,41} The term *embedded* commonly implies substitution of an additive or doped metal into sites such as cation vacancies of supports typified by metal oxides,³⁷ but this term is vague because the substitution can occur both at the surface and within the bulk of the support.⁴²

Some prior catalysis investigations acknowledge that subsurface platinum could contribute to reactivity, but the authors did not explicitly consider these sites in models (e.g., ref 43). Kraushofer et al.⁴⁴ reported rhodium clusters stabilized in the subsurface of single-crystal Fe₂O₃. They characterized both atomically dispersed rhodium on the surface and subsurface species formed from it by using XPS and He⁺ low-energy ion scattering complemented with DFT calculations. Our results are contrasted with those of Kraushofer et al.,⁴⁴ because we report a comparison of first-layer and second-layer metal catalysts that are both atomically dispersed and characterized by evidence of their structures under working catalytic conditions.

We posit that atomically dispersed platinum on MgO powder may be regarded as a prototypical catalyst for investigating the interconversions of noble metal structures with various metal–support interactions. We envision other noble metal–support combinations that illustrate new properties including trade-offs between catalyst stability, activity, and selectivity and perhaps structures that retain stability while providing better activity and selectivity.

■ ASSOCIATED CONTENT

SI Supporting Information

The Supporting Information is available free of charge at <https://pubs.acs.org/doi/10.1021/acs.jpcllett.2c00667>.

Experimental details, additional experimental results, description of computational methodology, Supporting Figures S1–S14 (TEM image and XRD pattern, IR and XANES spectra, O 1s XPS data, N₂ isotherms, phase diagrams, HERFD-XANES comparison, HAADF-STEM image, and stability of Pt/MgO₄₀₀ catalyst) and Supporting Tables S1 and S2 (BET surface areas and ¹²C harmonic approximation calculation and scaling) (PDF)

■ AUTHOR INFORMATION

Corresponding Authors

Coleman X. Kronawitter – Department of Chemical Engineering, University of California, Davis, California 95616, United States; orcid.org/0000-0002-1240-5027; Email: ckrona@ucdavis.edu

Simon R. Bare – Stanford Synchrotron Radiation Lightsource, SLAC National Accelerator Laboratory, Menlo Park, California 94025, United States; orcid.org/0000-0002-4932-0342; Email: srbare@slac.stanford.edu

Ambarish R. Kulkarni – Department of Chemical Engineering, University of California, Davis, California 95616, United States; orcid.org/0000-0001-9834-8264; Email: arkulkarni@ucdavis.edu

Bruce C. Gates – Department of Chemical Engineering, University of California, Davis, California 95616, United States; orcid.org/0000-0003-0274-4882; Email: bcbates@ucdavis.edu

Authors

Yizhen Chen – Department of Chemical Engineering, University of California, Davis, California 95616, United States

Rachita Rana – Department of Chemical Engineering, University of California, Davis, California 95616, United States

Zhennan Huang – Oak Ridge National Laboratory, Oak Ridge, Tennessee 37830, United States

Fernando D. Vila – Department of Physics, University of Washington, Seattle, Washington 98195, United States; orcid.org/0000-0002-6508-4896

Tyler Sours – Department of Chemical Engineering, University of California, Davis, California 95616, United States

Jorge E. Perez-Aguilar – Stanford Synchrotron Radiation Lightsource, SLAC National Accelerator Laboratory, Menlo Park, California 94025, United States

Xiao Zhao – Materials Sciences Division, Lawrence Berkeley National Laboratory, Berkeley and Department of Materials Science and Engineering, University of California, Berkeley, Berkeley, California 94720, United States; orcid.org/0000-0003-1079-664X

Jiyun Hong – Stanford Synchrotron Radiation Lightsource, SLAC National Accelerator Laboratory, Menlo Park, California 94025, United States

Adam S. Hoffman – Stanford Synchrotron Radiation Lightsource, SLAC National Accelerator Laboratory, Menlo Park, California 94025, United States; orcid.org/0000-0002-7682-4108

Xu Li – Hefei National Laboratory for Physical Sciences at the Microscale, National Synchrotron Radiation Laboratory, University of Science and Technology of China, Hefei, Anhui 230026, P. R. China

Chunyan Shang – Hefei National Laboratory for Physical Sciences at the Microscale, National Synchrotron Radiation Laboratory, University of Science and Technology of China, Hefei, Anhui 230026, P. R. China

Thomas Blum – University of California Irvine, Irvine, California 92697, United States

Jie Zeng – Hefei National Laboratory for Physical Sciences at the Microscale, National Synchrotron Radiation Laboratory, University of Science and Technology of China, Hefei, Anhui 230026, P. R. China; orcid.org/0000-0002-8812-0298

Miaofang Chi – Oak Ridge National Laboratory, Oak Ridge, Tennessee 37830, United States; orcid.org/0000-0003-0764-1567

Miquel Salmeron – Materials Sciences Division, Lawrence Berkeley National Laboratory, Berkeley and Department of Materials Science and Engineering, University of California, Berkeley, Berkeley, California 94720, United States; orcid.org/0000-0002-2887-8128

Complete contact information is available at: <https://pubs.acs.org/doi/10.1021/acs.jpcllett.2c00667>

Author Contributions

[○]Y.Z. and R.R. contributed equally to this work.

Notes

The authors declare no competing financial interest. Additional supporting research data (ASE database file and EXAFS fitting routines) for this article may be accessed on GitHub at https://github.com/kul-group/kul-repository/blob/main/repo_2022_JPCLE_Atatomically%20Dispersed%20Platinum/ and <https://github.com/kul-group/QuantEXAFS>, respectively.

■ ACKNOWLEDGMENTS

Y.C. and B.C.G. were supported by the U.S. Department of Energy (DOE), Office of Science, Basic Energy Sciences (BES)

grant DE-FG02-04ER15513. Stanford Synchrotron Radiation Lightsource (SSRL) of SLAC National Accelerator Laboratory is supported by BES under Contract No. DE-AC02-76SF00515. Co-ACCESS is supported by the BES Chemical Sciences, Geosciences, and Biosciences Division. C.X.K. and A.R.K. were supported by the DOE, Office of Science, BES grant DE-SC0020320. R.R. acknowledges support from the DOE (DE-SC0020320, for DFT calculations) and from Co-ACCESS. Z.H. was supported by the DOE BES, Chemical Sciences, Geosciences, and Biosciences Division. Electron microscopy was performed at the Oak Ridge National Laboratory Center for Nanophase Materials Sciences, which is a DOE Office of Science User Facility (T.B., M.C.). T.S. acknowledges support from the DOE (DE-SC0020320). X.Z. and M.S. were supported by the National Science Foundation grant number 1906014. The DFT and HERFD-XANES calculations were performed using the resources of the National Energy Research Scientific Computing Center, a DOE Office of Science User Facility located at Lawrence Berkeley National Laboratory, operated under Contract No. DE-AC02-05CH11231. XPS characterizations were performed at the Molecular Foundry supported by the DOE under Contract No. DE-AC02-05CH11231. The authors acknowledge Noah W. Felvey for help in the experiments.

REFERENCES

- (1) Liu, J. Catalysis by Supported Single Metal Atoms. *ACS Catal.* **2017**, *7* (1), 34–59.
- (2) Hulva, J.; Meier, M.; Bliem, R.; Jakub, Z.; Kraushofer, F.; Schmid, M.; Diebold, U.; Franchini, C.; Parkinson, G. S. Unraveling CO Adsorption on Model Single-Atom Catalysts. *Science* **2021**, *371* (6527), 375–379.
- (3) Chen, Y.; Sun, H. S.; Gates, B. C. Prototype Atomically Dispersed Supported Metal Catalysts: Iridium and Platinum. *Small* **2021**, *17* (16), 2004665.
- (4) Gates, B. C. Atomically Dispersed Supported Metal Catalysts: Seeing Is Believing. *Trends Chem.* **2019**, *1* (1), 99–110.
- (5) DeRita, L.; Resasco, J.; Dai, S.; Boubnov, A.; Thang, H. V.; Hoffman, A. S.; Ro, I.; Graham, G. W.; Bare, S. R.; Pacchioni, G.; Pan, X.; Christopher, P. Structural Evolution of Atomically Dispersed Pt Catalysts Dictates Reactivity. *Nat. Mater.* **2019**, *18* (7), 746–751.
- (6) Hoffman, A. S.; Debeve, L. M.; Zhang, S. J.; Perez-Aguilar, J. E.; Conley, E. T.; Justl, K. R.; Arslan, I.; Dixon, D. A.; Gates, B. C. Beating Heterogeneity of Single-Site Catalysts: MgO-Supported Iridium Complexes. *ACS Catal.* **2018**, *8* (4), 3489–3498.
- (7) Liu, L.; Zakharov, D.; Arenal, R.; Concepción, P.; Stach, E. A.; Corma, A. Evolution and Stabilization of Subnanometric Metal Species in Confined Space by In Situ TEM. *Nat. Commun.* **2018**, *9*, 574.
- (8) Duan, S.; Wang, R.; Liu, J. Stability Investigation of A High Number Density Pt₁/Fe₂O₃ Single-Atom Catalyst Under Different Gas Environments by HAADF-STEM. *Nanotechnology* **2018**, *29* (20), 204002.
- (9) Liu, L.; Meira, D. M.; Arenal, R.; Concepción, P.; Puga, A. V.; Corma, A. Determination of the Evolution of Heterogeneous Single Metal Atoms and Nanoclusters under Reaction Conditions: Which Are the Working Catalytic Sites? *ACS Catal.* **2019**, *9*, 10626–10639.
- (10) Moliner, M.; Gabay, J. E.; Kliewer, C. E.; Carr, R. T.; Guzman, J.; Casty, G. L.; Serna, P.; Corma, A. Reversible Transformation of Platinum Nanoparticles into Single Atoms inside High-Silica Chabazite Zeolite. *J. Am. Chem. Soc.* **2016**, *138* (48), 15743–15750.
- (11) Liu, L.; Corma, A. Metal Catalysts for Heterogeneous Catalysis: From Single Atoms to Nanoclusters and Nanoparticles. *Chem. Rev.* **2018**, *118* (10), 4981–5079.
- (12) Uzun, A.; Gates, B. C. Real-Time Characterization of Formation and Breakup of Iridium Clusters in Highly Dealuminated Zeolite Y. *Angew. Chem., Int. Ed.* **2008**, *47* (48), 9245–9248.
- (13) Chen, Y.; Rana, R.; Sours, T.; Vila, F. D.; Cao, S.; Blum, T.; Hong, J.; Hoffman, A. S.; Fang, C.-Y.; Huang, Z.; Shang, C.; Wang, C.; Zeng, J.; Chi, M.; Kronawitter, C. X.; Bare, S. R.; Gates, B. C.; Kulkarni, A. R. A Theory-Guided X-ray Absorption Spectroscopy Approach for Identifying Active Sites in Atomically Dispersed Transition-Metal Catalysts. *J. Am. Chem. Soc.* **2021**, *143* (48), 20144–20156.
- (14) Sarma, B. B.; Plessow, P. N.; Agostini, G.; Concepción, P.; Pfänder, N.; Kang, L.; Wang, F. R.; Studt, F.; Prieto, G. Metal-Specific Reactivity in Single-Atom Catalysts: CO Oxidation on 4d and 5d Transition Metals Atomically Dispersed on MgO. *J. Am. Chem. Soc.* **2020**, *142* (35), 14890–14902.
- (15) Sarma, B. B.; Agostini, G.; Farpón, M. G.; Marini, C.; Pfänder, N.; Prieto, G. Bottom-Up Assembly of Bimetallic Nanocluster Catalysts from Oxide-Supported Single-Atom Precursors. *J. Mater. Chem. A* **2021**, *9*, 8401–8415.
- (16) Khairallah, F.; Glisenti, A.; Natile, M. M.; Galenda, A. CuO/MgO Nanocomposites by Wet Impregnation: An XPS Study. *Surf. Sci. Spectra* **2012**, *19* (1), 23–29.
- (17) Denny, Y. R.; Firmansyah, T.; Gustiono, V.; Lee, S. S. Effect of Substrate Temperature on the Electronic Properties of MgO Thin Films on Si (100) Grown by Electron Beam Evaporation. *Key Eng. Mater.* **2020**, *841*, 243–247.
- (18) Hao, Y.; Liu, B.; Tian, L.; Li, F.; Ren, J.; Liu, S.; Liu, Y.; Zhao, J.; Wang, X. Synthesis of {111} Facet-Exposed MgO with Surface Oxygen Vacancies for Reactive Oxygen Species Generation in the Dark. *ACS Appl. Mater. Inter.* **2017**, *9* (14), 12687–12693.
- (19) Debeve, L. M.; Hoffman, A. S.; Yeh, A. J.; Runnebaum, R. C.; Shulda, S.; Richards, R. M.; Arslan, I.; Gates, B. C. Iridium Atoms Bonded to Crystalline Powder MgO: Characterization by Imaging and Spectroscopy. *J. Phys. Chem. C* **2020**, *124* (1), 459–468.
- (20) Newville, M. Larch: An Analysis Package for XAFS and Related Spectroscopies. *J. Phys.: Conf. Ser.* **2013**, *430*, No. 012007.
- (21) Kresse, G.; Hafner, J. Ab Initio Molecular Dynamics for Liquid Metals. *Phys. Rev. B: Condens. Matter Mater. Phys.* **1993**, *47*, 558–561.
- (22) Larsen, A. H.; Mortensen, J. J.; Blomqvist, J.; Castelli, I. E.; Christensen, R.; Dulak, M.; Friis, J.; Groves, M. N.; Hammer, B.; Hargus, C.; Hermes, E. D.; Jennings, P. C.; Jensen, P. B.; Kermode, J.; Kitchin, J. R.; Kolsbjerg, E. L.; Kubal, J.; Kaasbjerg, K.; Lysgaard, S.; Maronsson, J. B.; Maxson, T.; Olsen, T.; Pastewka, L.; Peterson, A.; Rostgaard, C.; Schiøtz, J.; Schütt, O.; Strange, M.; Thygesen, K. S.; Vegge, T.; Vilhelmsen, L.; Walter, M.; Zeng, Z.; Jacobsen, K. W. The Atomic Simulation Environment—A Python Library for Working with Atoms. *J. Phys.: Condens. Matter* **2017**, *29*, 273002.
- (23) Lym, J.; Wittreich, G. R.; Vlachos, D. G. A Python Multiscale Thermochemistry Toolbox (PMuTT) for Thermochemical and Kinetic Parameter Estimation. *Comput. Phys. Commun.* **2020**, *247*, 106864.
- (24) Lu, Y.; Wang, J.; Yu, L.; Kovarik, L.; Zhang, X.; Hoffman, A. S.; Gallo, A.; Bare, S. R.; Sokaras, D.; Kroll, T.; Dagle, V.; Xin, H.; Karim, A. M. Identification of the Active Complex for CO Oxidation over Single-Atom Ir-on-MgAl₂O₄ Catalysts. *Nat. Catal.* **2019**, *2* (2), 149–156.
- (25) Hoffman, A. S.; Sokaras, D.; Zhang, S. J.; Debeve, L. M.; Fang, C.-Y.; Gallo, A.; Kroll, T.; Dixon, D. A.; Bare, S. R.; Gates, B. C. High-Energy-Resolution X-ray Absorption Spectroscopy for Identification of Reactive Surface Species on Supported Single-Site Iridium Catalysts. *Chem.-Eur. J.* **2017**, *23*, 14760–14768.
- (26) Rehr, J. J.; Kas, J. J.; Prange, M. P.; Sorini, A. P.; Takimoto, Y.; Vila, F. Ab Initio Theory and Calculations of X-Ray Spectra. *C. R. Phys.* **2009**, *10*, 548–559.
- (27) Rehr, J. J.; Kas, J. J.; Vila, F. D.; Prange, M. P.; Jorissen, K. Parameter-Free Calculations of X-Ray Spectra with FEFF9. *Phys. Chem. Chem. Phys.* **2010**, *12*, 5503–5513.

(28) Qiao, B.; Wang, A.; Yang, X.; Allard, L. F.; Jiang, Z.; Cui, Y.; Liu, J.; Li, J.; Zhang, T. Single-Atom Catalysis of CO Oxidation Using Pt₁/FeO_x. *Nat. Chem.* **2011**, *3* (8), 634–641.

(29) Hoffman, A. S.; Fang, C.-Y.; Gates, B. C. Homogeneity of Surface Sites in Supported Single-Site Metal Catalysts: Assessment with Band Widths of Metal Carbonyl Infrared Spectra. *J. Phys. Chem. Lett.* **2016**, *7* (19), 3854–3860.

(30) Ding, K.; Gulec, A.; Johnson, A. M.; Schweitzer, N. M.; Stucky, G. D.; Marks, L. D.; Stair, P. C. Identification of Active Sites in CO Oxidation and Water-Gas Shift over Supported Pt Catalysts. *Science* **2015**, *350*, 189–192.

(31) Maurer, F.; Jelic, J.; Wang, J.; Gänzler, A.; Dolcet, P.; Wöll, C.; Wang, Y.; Studt, F.; Casapu, M.; Grunwaldt, J.-D. Tracking the Formation, Fate and Consequence for Catalytic Activity of Pt Single Sites on CeO₂. *Nat. Catal.* **2020**, *3* (10), 824–833.

(32) Xu, J.; Yates, J. T. Terrace Width Effect on Adsorbate Vibrations: A Comparison of Pt(335) and Pt(112) for Chemisorption of CO. *Surf. Sci.* **1995**, *327*, 193–201.

(33) Dessal, C.; Len, T.; Morfin, F.; Rousset, J.-L.; Aouine, M.; Afanasiev, P.; Piccolo, L. Dynamics of Single Pt Atoms on Alumina during CO Oxidation Monitored by Operando X-Ray and Infrared Spectroscopies. *ACS Catal.* **2019**, *9*, 5752–5759.

(34) Abbet, S.; Heiz, U.; Hakkinen, H.; Landman, U. CO Oxidation on a Single Pd Atom Supported on Magnesia. *Phys. Rev. Lett.* **2001**, *86*, 5950–5953.

(35) Amsler, J.; Sarma, B. B.; Agostini, G.; Prieto, G.; Plessow, P. N.; Studt, F. Prospects of Heterogeneous Hydroformylation with Supported Single Atom Catalysts. *J. Am. Chem. Soc.* **2020**, *142*, 5087–5096.

(36) Gil, W.; Trzeciak, A. M. N-Heterocyclic Carbene–Rhodium Complexes as Catalysts for Hydroformylation and Related Reactions. *Coord. Chem. Rev.* **2011**, *255*, 473–483.

(37) Guo, X.; Fang, G.; Li, G.; Ma, H.; Fan, H.; Yu, L.; Ma, C.; Wu, X.; Deng, D.; Wei, M.; Tan, D.; Si, R.; Zhang, S.; Li, J.; Sun, L.; Tang, Z.; Pan, X.; Bao, X. Direct, Nonoxidative Conversion of Methane to Ethylene, Aromatics, and Hydrogen. *Science* **2014**, *344* (6184), 616–619.

(38) Yao, Y.; Hu, S.; Chen, W.; Huang, Z.-Q.; Wei, W.; Yao, T.; Liu, R.; Zang, K.; Wang, X.; Wu, G.; Yuan, W.; Yuan, T.; Zhu, B.; Liu, W.; Li, Z.; He, D.; Xue, Z.; Wang, Y.; Zheng, X.; Dong, J.; Chang, C.-R.; Chen, Y.; Hong, X.; Luo, J.; Wei, S.; Li, W.-X.; Strasser, P.; Wu, Y.; Li, Y. Engineering the Electronic Structure of Single Atom Ru Sites via Compressive Strain Boosts Acidic Water Oxidation Electrocatalysis. *Nat. Catal.* **2019**, *2* (4), 304–313.

(39) Aich, P.; Wei, H.; Basan, B.; Kropf, A. J.; Schweitzer, N. M.; Marshall, C. L.; Miller, J. T.; Meyer, R. Single-Atom Alloy Pd-Ag Catalyst for Selective Hydrogenation of Acrolein. *J. Phys. Chem. C* **2015**, *119*, 18140–18148.

(40) Thum, L.; Riedel, W.; Milojevic, N.; Guan, C.; Trunschke, A.; Dinse, K.-P.; Risse, T.; Schomäcker, R.; Schlögl, R. Transition-Metal-Doping of CaO as Catalyst for the OCM Reaction, a Reality Check. *Front. Chem.* **2022**, *10*, 768426–768426.

(41) Nilius, N.; Freund, H.-J. Activating Nonreducible Oxides via Doping. *Acc. Chem. Res.* **2015**, *48*, 1532–1539.

(42) Sudrajat, H.; Fadlallah, M. M.; Tao, S.; Kitta, M.; Ichikuni, N.; Onishi, H. Dopant Site in Indium-Doped SrTiO₃ Photocatalysts. *Phys. Chem. Chem. Phys.* **2020**, *22* (34), 19178–19187.

(43) Tang, W.; Hu, Z.; Wang, M.; Stucky, G. D.; Metiu, H.; McFarland, E. W. Methane Complete and Partial Oxidation Catalyzed by Pt-Doped CeO₂. *J. Catal.* **2010**, *273* (2), 125–137.

(44) Kraushofer, F.; Resch, N.; Eder, M.; Rafsanjani-Abbasi, A.; Tobisch, S.; Jakub, Z.; Franceschi, G.; Riva, M.; Meier, M.; Schmid, M.; Diebold, U.; Parkinson, G. S. Surface Reduction State Determines Stabilization and Incorporation of Rh on α -Fe₂O₃(1 $\bar{1}$ 02). *Adv. Mater. Interfaces* **2021**, *8* (8), 2001908.